Reconstruction algorithm for atomic-resolution holography using translational symmetry

Tomohiro Matsushita,* Fang Zhun Guo, and Motohiro Suzuki
Japan Synchrotron Radiation Research Institute (JASRI), SPring-8, 1-1-1 Kouto, Sayo-cho, Sayo-gun Hyogo 679-5198, Japan

Fumihiko Matsui and Hiroshi Daimon
Nara Institute of Science and Technology (NAIST), 8916-5 Takayama, Ikoma, Nara 630-0192 Japan

Kouichi Hayashi
Institute for Materials Research, Tohoku University, Sendai 980-8577, Japan

(Received 12 March 2008; revised manuscript received 4 August 2008; published 29 October 2008)

The most widely used methods for reconstructing three-dimensional atomic arrangements from a photoelectron hologram and an x-ray fluorescence hologram are based on an integral kernel, for example, the Fourier transformation. These methods require many holograms that are recorded using multiple energies since the Fourier transformation requires an infinite integral interval. Therefore, it is difficult to reconstruct an atomic arrangement from a single-energy hologram. In order to accomplish to reconstruct the three-dimensional atomic arrangement from a single-energy hologram, we have proposed a scattering pattern extraction algorithm using the maximum-entropy method (SPEA-MEM) for photoelectron holography. In this paper, we also describe the application of this algorithm to x-ray fluorescence holography. We have succeeded in reconstructing 58 Au atoms from a single-energy x-ray fluorescence hologram that we have measured. However, artifacts have been observed in the reconstructed image. This is due to the long coherent length and the mean-free path of the x rays. Hence, we have incorporated crystal translational symmetry into SPEA-MEM to solve this problem. We have applied this algorithm to an x-ray fluorescence hologram of Au and a photoelectron hologram of Cu that we have measured. We have succeeded in reconstructing a very clear atomic arrangement with an accuracy of 0.01 nm in three-dimensional real space for both holograms.

DOI: 10.1103/PhysRevB.78.144111 PACS number(s): 42.40.−i, 61.05.jp, 78.70.En

I. INTRODUCTION

In recent years, photoelectron holography, Auger electron holography, and x-ray fluorescence holography have been developed to study atomic arrangement. Holography is a method for recording a three-dimensional image on a two-dimensional image using a coherent waveform. Holography was originally proposed by Gabor[1] for the electron microscope. Szöke[2] has pointed out that atomic-resolution holography can be realized by utilizing a wave emitted from an atom, such as a characteristic x ray, photoelectron, and Auger electron. The emitted wave is scattered by the surrounding atoms, and an interference pattern between the direct wave and the scattered waves is observed in the angular intensity distribution. The angular distribution is interpreted as a hologram that records the three-dimensional atomic arrangement. Barton has proposed a numerical algorithm based on the Fourier transform[3–5] to reconstruct a three-dimensional atomic arrangement from a photoelectron hologram (PEH). However, the atomic image reconstructed by this method was unclear.[3–6] In principle, it is quite difficult to reconstruct an atomic arrangement from a single-energy hologram. This is because the integral kernel of the Fourier transform requires an infinite integration interval, and it is necessary to measure as many holograms as possible with different kinetic energies. In addition, the Fourier transform is not a good approximation for the electron hologram since the electron wave scattered by an atom is quite different from the *s* wave. To date, several correction methods based on the multienergy format have been proposed for the PEH.[4,7–23]

In the case of the x-ray fluorescence hologram (XFH), the effects of the asymmetry of the scattered wave are not serious. Several experimental methods and algorithms based on the Fourier transform have been studied.[24–32] In order to obtain the multienergy format, an inverse x-ray fluorescence hologram (IXFH) has been developed. The algorithm that was developed based on the Fourier transform and the multienergy format succeeded in reconstructing an atomic image with subangstrom resolution. However, considerable time was required to measure the multienergy of the IXFH. It is still difficult to reconstruct from a single-energy XFH or IXFH because the Fourier transform requires an infinite integral interval.

The Fourier transform cannot be expanded because its basis function cannot be changed. Recently, Marchesini *et al.*[28] have proposed an iterative image deconvolution method to improve the atomic image for fluorescence holography and reported the application of a theoretically calculated hologram using a small atomic cluster. Even when their method is utilized, the application of an actual XFH may be difficult because they have directly utilized the electron density, and its application will require the use of a fine three-dimensional real-space mesh (voxel) in the calculation in order to describe the density of the inner-shell electrons. In addition, as shown later, radial correction in the reconstruction algorithm is not introduced. In this case, the intensity of the atomic image decreases with an increase in the distance from the emitter atom.

We have proposed a scattering pattern extraction algorithm using the maximum-entropy method (SPEA-MEM) (Ref. 33–35) for the analysis of PEH and Auger electron hologram (AEH). This algorithm is not based on the integral kernel, and it can reconstruct the atomic arrangement from a

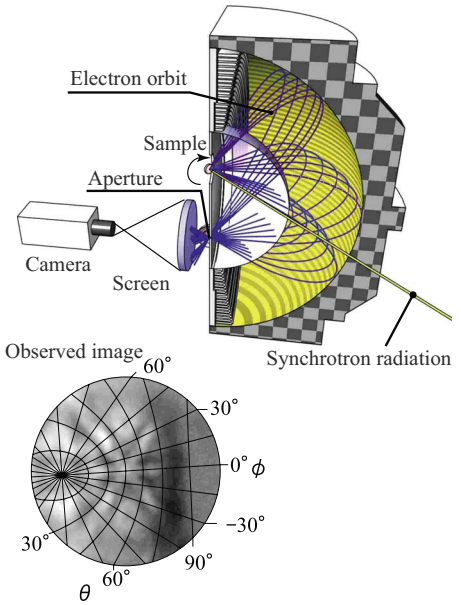

FIG. 1. (Color online) Schematic view of the experimental setup and two-dimensional display-type analyzer. Angular distribution without distortion is directly projected onto the screen. An example of the observed image is shown in the figure.

single-energy hologram. We already tested the algorithm by using a PEH of Si(001) (Ref. 34) and an AEH of Cu(001).[35] In this paper, we propose to apply the SPEA-MEM to the IXFH (XFH). The validity and accuracy of the algorithm are examined using an experimental IXFH of Au while comparing with an experimental PEH of Cu(001). Furthermore, we report an algorithm in which the symmetry operations are incorporated into the SPEA-MEM. This algorithm was tested using both the IXFH of Au and the PEH of Cu. It dramatically improves the clarity of the atomic image.

II. EXPERIMENT

A. Photoelectron holography

The Cu(001) crystal was measured at BL25SU of the SPring-8 synchrotron-radiation facility. High-energy resolution and circularly polarized light in the range of 0.2–2 keV were available. The Cu(001) surface was cleaned by annealing. Reflection high-energy electron diffraction (RHEED), and x-ray photoemission spectroscopy were employed to examine whether the surface was cleaned by this process. The PEH of Cu(001) was measured using a two-dimensional display-type analyzer.[36–38] A schematic view of the experimental setup is shown in Fig. 1. The angular distribution of $\pm 56°$ is projected onto the screen of the analyzer, and it is measured with a charge-coupled-device (CCD) camera. In this experiment, synchrotron radiation entered the sample in a direction normal to the surface. Seventy-two hologram images were measured by rotating the sample. In this experimental setup, the condition of the crystal and the polarized light did not change because the light was circularly polarized. A 2π sr PEH was developed from the measured images. Figure 2 shows the measured Cu(001) PEH. The lines in the figure indicate the Kikuchi band. The reciprocal-lattice vectors can be deduced from these patterns.

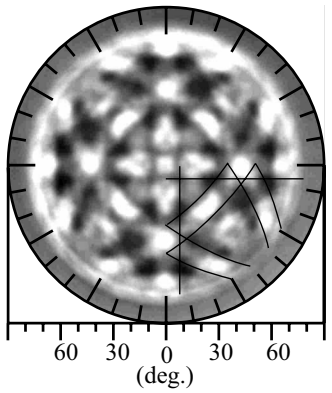

FIG. 2. Measured Cu(001) PEH. The kinetic energy of the photoelectron is 818 eV, and the initial state is the Cu $3p$ state. The lines in the figure indicate the Kikuchi band.

B. X-ray holography

The measured sample was a single crystal of Au (001). The experiment was performed at BL39XU of SPring-8. The incident x-ray energy was 12.0 keV. We used a circularly polarized x-ray beam generated by a diamond x-ray phase retarder[39,40] for simplicity of data analysis. The scattering pattern function depends on the direction of the electric-field vector of the x rays. The number of parameters for averaging can be significantly reduced for nonpolarized or circularly polarized x rays since the direction of the electric-field vector varies every moment in these polarization states.

The Au $L\alpha$ (9.712 keV) x-ray fluorescence was analyzed and focused by a cylindrical LiF crystal. The focused strong x-ray fluorescence was detected by an avalanche photodiode. The fluorescence intensities were measured as a function of the azimuthal angle ϕ and polar angle θ within the ranges of $0 \leq \phi \leq 360°$ and $0 \leq \theta \leq 70°$. The count rate of the x-ray fluorescence was about 5×10^5 cps.

The measured hologram was extended to 4π sr images by considering the symmetry of the Au crystal. The image is shown in Fig. 3. The observed lines and curves in the figure indicate standing-wave lines.

III. BASIC ALGORITHM

The angular distribution of the photoelectron or Auger electron is given by[41]

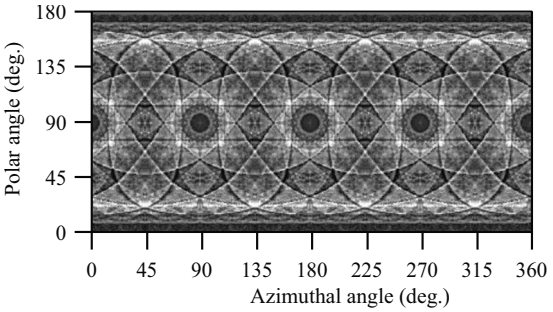

FIG. 3. Measured Au(001) IXFH. The photon energy is 12 keV.

$$I_e(\mathbf{k}) = \sum_L \left| \Phi_L(\mathbf{k}) + \sum_h \Psi_L(\mathbf{k},\mathbf{a}_h) \right|^2, \quad (1)$$

where $\mathbf{k}$ and $\mathbf{a}_h$ represent a wave-number vector and a position vector of the scatterer atom, respectively. h is an integer index for the scatterer atom. $\Phi_L(\mathbf{k})$ is the wave function of the excited electron, and L is an index of the type of the excited electron wave. $\Psi_L(\mathbf{k},\mathbf{a}_h)$ denotes the scattered wave function caused by the atom located at $\mathbf{a}_h$. The scattered wave function is given by[41]

$$\Psi_L(\mathbf{k},\mathbf{a}) = \frac{e^{i(|\mathbf{k}||\mathbf{a}|-\mathbf{k}\mathbf{a})}}{|\mathbf{a}|} f_L^e(\mathbf{k},\mathbf{a}), \quad (2)$$

where $f_L^e(\mathbf{k},\mathbf{r})$ is the scattering factor for the electron and is a function of a complex variable.

Here we repeat the basic expressions for the electron hologram from Ref. 35 for clarity. The intensity of the excited wave function is given by

$$I_0(\mathbf{k}) = \sum_L |\Phi_L(\mathbf{k})|^2, \quad (3)$$

and the electron hologram function is defined as

$$\chi_e(\mathbf{k}) = I_e(\mathbf{k}) - I_0(\mathbf{k}), \quad (4)$$

$$= \sum_h \sum_L (|\Psi_L(\mathbf{k},\mathbf{a}_h)|^2 + 2\,\mathrm{Re}[\Phi_L^*(\mathbf{k})\Psi_L(\mathbf{k},\mathbf{a}_h)]). \quad (5)$$

When a scattering pattern function is defined as

$$t_e(\mathbf{k},\mathbf{a}) = |\mathbf{a}| \sum_L (|\Psi_L(\mathbf{k},\mathbf{a})|^2 + 2\,\mathrm{Re}[\Phi_L^*(\mathbf{k})\Psi_L(\mathbf{k},\mathbf{a})]), \quad (6)$$

the electron hologram function is given by

$$\chi_e(\mathbf{k}) = \sum_h \frac{t_e(\mathbf{k},\mathbf{a}_h)}{|\mathbf{a}_h|}. \quad (7)$$

It should be noted that the factor $|\mathbf{a}|$ in Eq. (6) is for the reconstruction of the atomic image as described later.

In the case of the XFH, the hologram χ_p is given by[42]

$$\chi_p(\mathbf{k}) = \left| \Phi_0(\mathbf{k}) + \int \frac{e^{i(|\mathbf{k}||\mathbf{r}|-\mathbf{k}\mathbf{r})}}{|\mathbf{r}|} f_p(\mathbf{k},\mathbf{r})\rho(\mathbf{r}) d^3\mathbf{r} \right|^2 - |\Phi_0|^2, \quad (8)$$

where ρ is the electronic charge-density distribution and $f_p(\mathbf{k},\mathbf{r})$ is the scattering factor of the x ray.

When the electron density is described as

$$\rho(\mathbf{r}) = \sum_h \rho'(\mathbf{r}-\mathbf{a}_h), \quad (9)$$

$$\Psi(\mathbf{k},\mathbf{a}) = \int \frac{e^{i(|\mathbf{k}||\mathbf{r}|-\mathbf{k}\mathbf{r})}}{|\mathbf{r}|} f_p(\mathbf{k},\mathbf{r})\rho'(\mathbf{r}-\mathbf{a}) d^3\mathbf{r}, \quad (10)$$

where ρ' is the electron density of each atom. When the scattering pattern function of XFH is defined as

$$t_p(\mathbf{k},\mathbf{a}) = |\mathbf{a}|(|\Psi(\mathbf{k},\mathbf{a})|^2 + 2\,\mathrm{Re}[\Phi_0^*(\mathbf{k})\Psi(\mathbf{k},\mathbf{a})]), \quad (11)$$

the hologram function is given by Eq. (7).

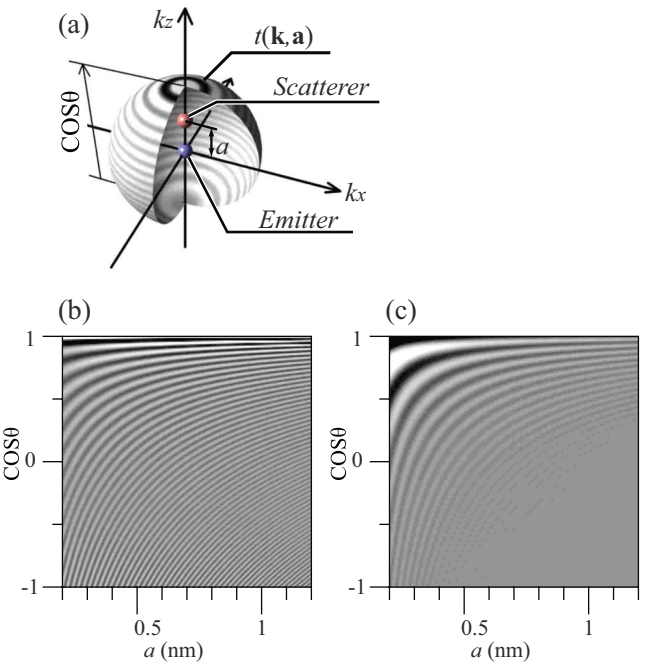

FIG. 4. (Color online) (a) Schematic view of the geometry of the scattering pattern function. (b) Scattering pattern function of an electron caused by the Cu atom. The kinetic energy is 818 eV. (c) Scattering pattern function of an x ray caused by the Au atom. The photon energy is 12 keV.

The reconstruction algorithm based on Fourier transform used to calculate the wave field U in the real space[3,4,28] is

$$U(\mathbf{r}') = \frac{1}{\Omega} \int_\sigma \eta^{\{-1\}}(\mathbf{r}',\mathbf{k}) \chi(\mathbf{k}) d^3\mathbf{k}, \quad (12)$$

$$\eta^{\{-1\}}(\mathbf{r}',\mathbf{k}) = |\mathbf{r}'| \mathrm{Re}[e^{-i(|\mathbf{k}||\mathbf{r}'|-\mathbf{k}\mathbf{r}')}], \quad (13)$$

where σ is the measured region in k space, Ω the volume of σ. $U(\mathbf{r})$ is an atomic distribution function, and $\chi(\mathbf{k})$ is the hologram function. Sometimes an additional factor $f^{\{-1\}}$ is included in $\eta^{\{-1\}}$ to compensate for the aberration or distortion produced by f. From a qualitative standpoint, when the volume Ω increased, the reliability of the atomic image becomes higher. In the case of a multienergy IXFH, the atomic image is successfully reconstructed by using this equation. However, in the case of the electron hologram, this integral kernel is not effective since the scattering function $f_L^e(\mathbf{k},\mathbf{a})$ is the function of a complex variable, and the imaginary part is not negligible. In the case of a single-energy hologram of XFH (IXFH) or PEH, the reconstructed atomic image using Eq. (12) is distorted and has artifact, because the measured volume Ω is quite limited.

We now describe the developed algorithm.[35] Figure 4 shows the scattering pattern function $t(\mathbf{k},\mathbf{a})$ of the PEH and XFH. In the case of the PEH, a strong forward-focusing peak appears around the angle $\cos\theta=1$. Further, the frequency of the intensity modulation around $\cos\theta=1$ differs from that of $e^{i(|\mathbf{k}||\mathbf{r}|-\mathbf{k}\mathbf{r})}$ because of the influence of the scattering factor. In the case of the XFH, the scattering pattern function is negative at $\cos\theta=1$. The frequency difference between the inten-

sity modulation and $e^{i(|\mathbf{k}||\mathbf{r}|-\mathbf{kr})}$ is small. However, the amplitude of the function decreases with decreasing cos θ and is not perfectly equal to the function $e^{i(|\mathbf{k}||\mathbf{r}|-\mathbf{kr})}$. In order to reconstruct the arrangement accurately, we select the scattering pattern function $t(\mathbf{k},\mathbf{a})$ as the basis function. The scattering pattern function is not orthogonal. Therefore, the integral kernel is not effective.

We extended Eq. (7) to the following equation that describes the hologram function:

$$\chi(\mathbf{k}) = \int g(\mathbf{a})t(\mathbf{k},\mathbf{a})d^3\mathbf{a}, \tag{14}$$

$$g(\mathbf{a}) = \sum_h \frac{\delta(\mathbf{a}-\mathbf{a}_h)}{|\mathbf{a}|}. \tag{15}$$

Here, $|\mathbf{a}|g(\mathbf{a})$ describes a three-dimensional atomic distribution function. The problem of reconstructing a three-dimensional atomic arrangement is reduced to the calculation of the function $g(\mathbf{a})$ from the hologram function $\chi(\mathbf{k})$.

In order to treat the three-dimensional atomic distribution function and the hologram function realistically, we introduced a three-dimensional mesh (voxel) or a two-dimensional mesh (pixel) for the representation of the functions $g(\mathbf{a})$ and $\chi(\mathbf{k})$. The above expression is modified as follows:

$$\chi(\mathbf{k}_i) = \sum_j g(\mathbf{a}_j)t(\mathbf{k}_i,\mathbf{a}_j)\Delta V_j, \tag{16}$$

where $\mathbf{k}_i$ and $\mathbf{a}_j$ are the vectors of the ith pixel of k space and the jth voxel of real space, respectively. ΔV_j represents the volume of the jth voxel of real space.

The expected spatial resolution of the PEH and the XFH is about 0.02–0.07 nm.[26,29,33] The voxel that is finer than the spatial resolution is necessary for Eq. (16). When ± 1 nm space is divided by 0.01 nm mesh, the number of voxels is 8×10^6. The number of sampling points of the single-energy hologram with 1 deg^2 mesh is about 3×10^4. Therefore, the number of unknown variables in this case is much greater than in that of the observed data. It cannot be solved by the simple gradient method. If the sampling point of hologram becomes more the same number of the voxel by using the multienergy format, it may be possible to solve Eq. (16) by using the simple gradient method. However, the very long measurement time is necessary.

In the case of the single-energy hologram, in order to calculate the function g, we must take into account the characteristics of the function g and the information theory. The function g is non-negative and is zero in most places. Therefore, the maximum-entropy method is quite effective. We used the iterative-scaling algorithm of the maximum-entropy method. The entropy[43] is defined as

$$S = -\sum_j g^{(n)}(\mathbf{a}_j)\ln\frac{g^{(n)}(\mathbf{a}_j)}{g^{(n-1)}(\mathbf{a}_j)} - \lambda C, \tag{17}$$

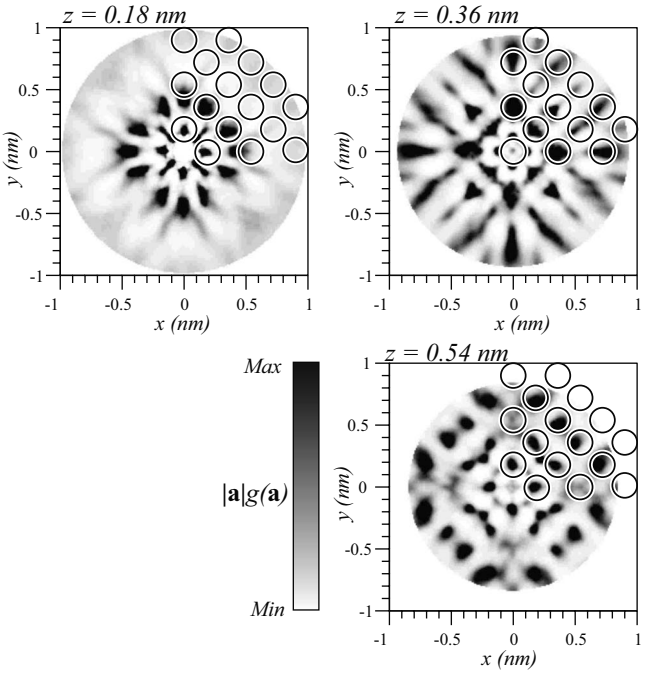

FIG. 5. Atomic images reconstructed from an experimental single-energy PEH of Cu(001). Each image is a cross section of the volume image at z=0, 0.18, and 0.36 nm. The darkness is proportional to the function $|\mathbf{a}|g(\mathbf{a})$. The circles show the expected position of the atoms.

$$C = \frac{1}{N}\sum_i \frac{\left|\chi(\mathbf{k}_i) - \sum_j g^{(n-1)}(\mathbf{a}_j)t(\mathbf{k}_i,\mathbf{a}_j)\Delta V_j\right|^2}{\sigma_i^2} - 1, \tag{18}$$

where n is an index for iteration and σ_i is the standard deviation of the noise. The entropy is maximized to obtain the real-space voxel, i.e., the three-dimensional real-space image. This algorithm is a common approach to reconstruct the atomic-resolution hologram, e.g., XFH, IXFH, PEH, and AEH.

In order to estimate the effectiveness of the algorithm, we have utilized a measured PEH of Cu(001) with a kinetic energy of 818 eV and a measured IXFH of Au with a photon energy of 12 keV. Figures 5 and 6 show the images reconstructed from the PEH of Cu and the IXFH of Au, respectively. In the case of the PEH, a clear atomic image is reconstructed. Since the region of the measured PEH is 2π sr ($z>0$) in size, the atomic image is also reconstructed in the $z>0$ region. The total number of atoms in the atomic image in three-dimensional space is 93.

In the case of the IXFH, we have succeeded in reconstructing the atomic image by using the SPEA-MEM. Since we use the IXFH in 4π sr, the atomic image is reconstructed in both the regions of $z\geq 0$ and $z<0$. The number of reconstructed atoms is 58 in three-dimensional real space, which is less than the number for the PEH. There are some artifacts present and there is also some amount of deterioration in the atomic images. This probably occurs due to the difference in the mean-free path of the electron and x ray. In the case of the PEH, the atomic cluster size is of nanometer order due to

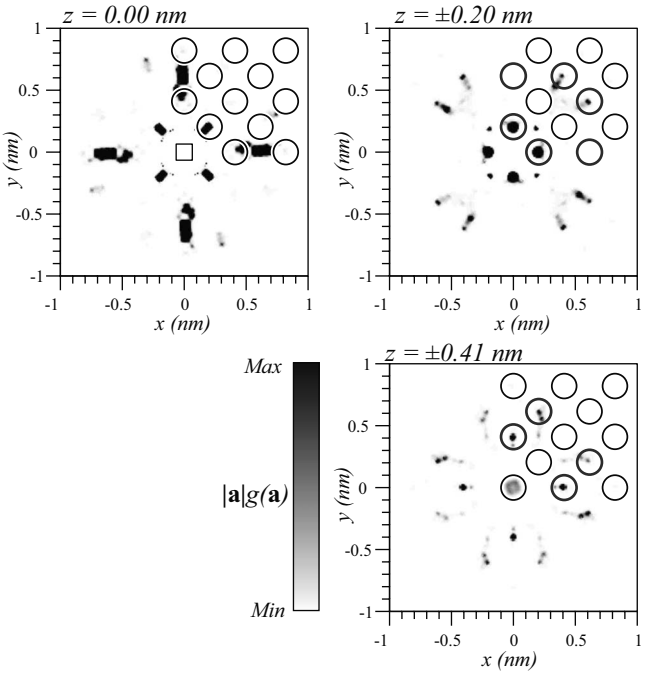

FIG. 6. Atomic images reconstructed from an experimental single-energy XFH of Au. Each image is a cross section of the volume image at z=0, ±0.20, and ±0.41 nm. The darkness is proportional to the function $|\mathbf{a}|g(\mathbf{a})$. The circles show the expected position of the atoms.

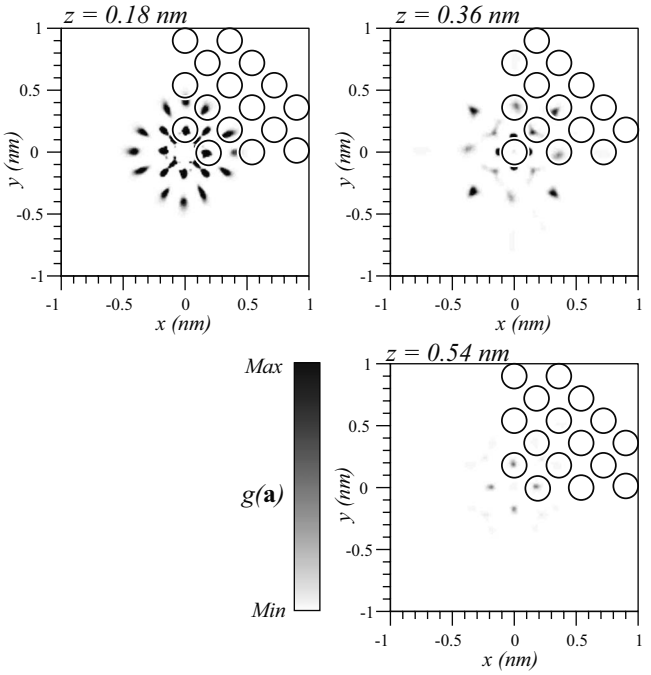

FIG. 7. Atomic images reconstructed from an experimental single-energy PEH of Cu(001) using the scattering pattern function without the factor $|\mathbf{a}|$. Each image shows a cross section of the volume image at z=0, 0.18, and 0.36 nm. The darkness is proportional to the function $g(\mathbf{a})$.

the mean-free path of the electron. Therefore, the size utilized in the calculation is fitted to that of the PEH. In the case of the XFH and IXFH, the atomic cluster size is quite large because of the weak absorption of x rays and the long coherent length. Therefore, the holographic pattern caused by distant atoms may cause the artifacts.

We would like to mention that the factor $|\mathbf{a}|$ in the scattering pattern function $t(\mathbf{k},\mathbf{a})$ is important for the reconstruction of the atomic image. When the scattering pattern matrix without the factor $|\mathbf{a}|$

$$\hat{t}(\mathbf{k},\mathbf{a}) = |\Psi(\mathbf{k},\mathbf{a})|^2 + 2\,\mathrm{Re}[\Phi_0^*(\mathbf{k})\Psi(\mathbf{k},\mathbf{a})] \tag{19}$$

is adopted, we obtain an atomic image as shown in Fig. 7. The image is clear only near the emitter atom; however, for distant atoms the clarity decreases significantly. This is caused by the asymmetry of the matrix element. Since the amplitude of the matrix element $\hat{t}(\mathbf{k},\mathbf{a})$ decreases with an increase in the distance from the emitter, the gradient of the sum of the squares $\partial C/\partial g(\mathbf{a}_j)$ for a distant atom has a small value. Therefore, the $g(\mathbf{a}_j)$ for distant atoms becomes small and the clarity of the image for distant atoms decreases significantly.

IV. EXTENDED ALGORITHM WITH TRANSLATIONAL SYMMETRY OPERATION

Information about the unit vector can be easily obtained by other methods, such as LEED, RHEED, and x-ray diffraction. Translational symmetry information is also extracted from the experimental hologram by using the Kikuchi pattern in the PEH or AEH, Kossel pattern in the XFH, and x-ray standing-wave pattern in the IXFH. However, even if the unit vector is measured, it is not possible to determine the atomic position. If information on the translational symmetry of the crystal is utilized by the reconstruction algorithm of the holography, the improvement of the atomic image can be expected. Some algorithms were studied in the XFH field,[44,45] and they are based on the Fourier series for the electron density of the unit cell. Here, we propose another extended reconstruction algorithm. We added the following calculation to the SPEA-MEM after each iteration calculation:

$$g(\mathbf{r}) = \sum_{|\mathbf{R}|<R_a} \frac{|\mathbf{r}+\mathbf{R}|}{|\mathbf{r}|} w(\mathbf{R}) g(\mathbf{r}+\mathbf{R}), \tag{20}$$

$$\mathbf{R} = l\hat{\mathbf{a}}_1 + m\hat{\mathbf{a}}_2 + n\hat{\mathbf{a}}_3, \tag{21}$$

where $\hat{\mathbf{a}}_n$ represents the unit vector of the crystal, R_a is the radius for the average operation, and w is a weight function. The unit-cell vector $\hat{\mathbf{a}}_n$ can be estimated by LEED, RHEED, the Kikuchi pattern, XRD, Kossel pattern, x-ray standing-wave pattern, etc. There are many ways to select $w(\mathbf{R})$. When $w(\mathbf{R})=\delta(\mathbf{R})$ is selected, the effect of the translational symmetry disappears. The effect of the translational symmetry operation can be controlled by careful selection of $w(\mathbf{R})$.

Here, we describe a case in which the effect of the translational symmetry operation is small. In this case, the weight function is given by

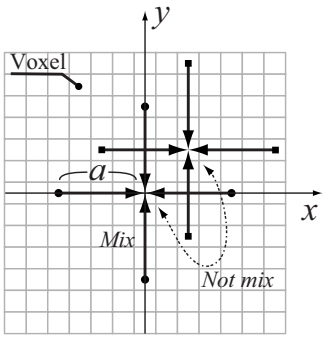

FIG. 8. Schematic view of mixture of voxels by translational symmetry.

$$w(\mathbf{R}) = \begin{cases} 1/C: & |\mathbf{R}| = 0 \\ v/C: & |\mathbf{R}| = \hat{a} \text{ (unit cell size)}, \\ 0: & \text{Others} \end{cases} \quad (22)$$

where v and C are the weight value and normalization parameter, respectively. The voxel value is mixed only with that of the neighboring unit cell. The schematic is shown in Fig. 8. In the case of the face-centered cubic (FCC) structure, the voxel located at the (0,0,1) position mixes with the voxels located at $(0,0,1\pm1)$,$(0,\pm1,1)$, $(\pm1,0,1)$. However, it does not mix with (1/2, 1/2, 0). Even with such an imperfect mixture, the atomic arrangement can be reconstructed clearly.

The result of the application of translational symmetry to the PEH of Cu, and the IXFH of Au are shown in Figs. 9 and 10, respectively. It can be observed that the atomic image has improved clearly. The shape of the atomic image becomes

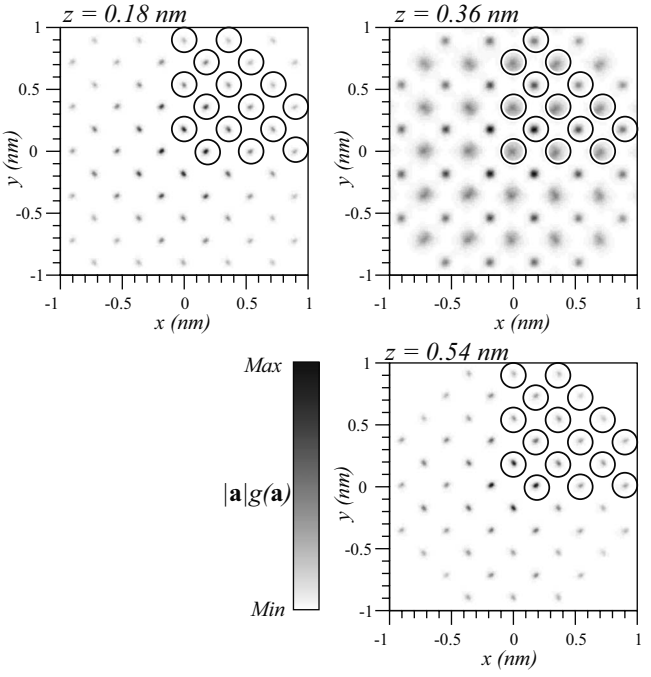

FIG. 9. Atomic image reconstructed from the experimental single-energy PEH of Cu(001) using the SPEA-MEM with the translational symmetry operation.

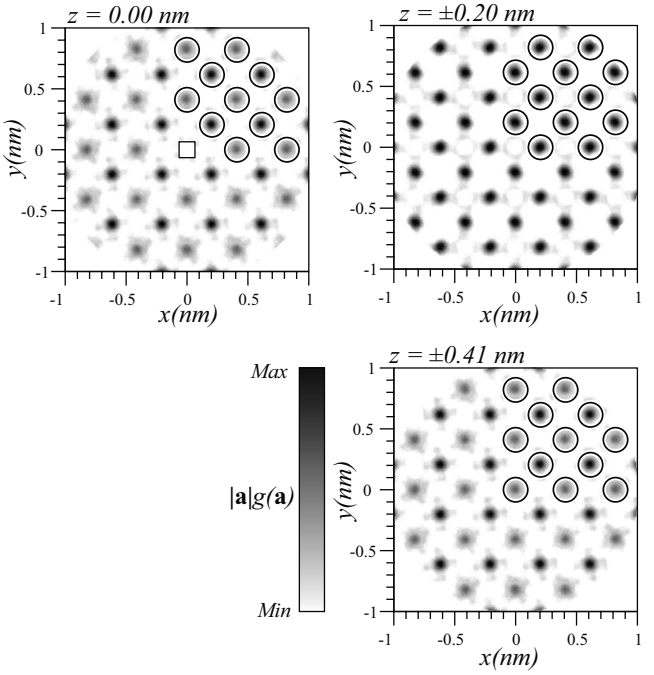

FIG. 10. Reconstructed atomic image from the experimental single-energy IXFH of Au by using the SPEA-MEM with the translational symmetry operation.

spherical. Although there is no mixing between the atomic image of (0, 0, 1) and that of (1/2, 1/2, 0), each atomic image is reproduced in its exact location. Therefore, the translational mixing method is quite effective in atomic image reconstruction.

When the perfect mixture for an FCC lattice using a set of primitive unit vectors

$$w(\mathbf{R}) = \begin{cases} 1/C: & |\mathbf{R}| = 0 \\ v/C: & |\mathbf{R}| = \hat{a}/\sqrt{2} \text{ (}\hat{a}\text{: unit cell size)}, \\ 0: & \text{Others} \end{cases} \quad (23)$$

is adopted, the clarity of the atomic image increases. We would like to mention that the atoms located not only at the corners of the unit cell but also those located in it are clearly reconstructed by using the translational symmetry operation of the unit cell vector.

V. CONCLUSION

We have developed the SPEA-MEM in order to apply it to x-ray holography. We have succeeded in reconstructing 58 atomic images from the experimentally observed IXFH of Au. However, some atomic images are missing. We have also extended the SPEA-MEM algorithm using the translational symmetry operation and tested it by using the experimentally observed PEH of Cu and IXFH of Au. The atomic images are successfully reconstructed from both holograms. The reconstructed atomic image is quite clear with almost no artifacts. This algorithm is effective, and practicable, since there are many ways to measure the translational vector. In this paper, the case of a bulk structure is introduced. It is

possible to apply the algorithm to a surface or an interfacial surface when the coefficients for the vertical translational symmetry in Eq. (22) are changed to zero. The SPEA-MEM with the translational symmetry enables the determination of a bulk structure around an individual atomic site or impurity by selecting the initial state dependent on the atomic species and chemical state. By selecting the core level of an adsorbate, it is also possible to investigate the surface structure. However, the translational operation algorithm cannot be applied to a case where the translational symmetry is locally broken around the emitter, for example, the local distortion caused by the impurity and adsorptions that do not form the translational symmetry. Even with these drawbacks, it is anticipated that the SPEA-MEM with the translational symmetry operation will become a powerful tool for determining the positions of atomic nuclei around particular target atomic sites.

ACKNOWLEDGMENTS

We thank T. Kinoshita, T. Muro, and T. Nakamura for their help with the PEH experiment at BL25SU. We are also grateful to A. Agui and A. Yoshigoe. This study was performed with the approval of the Japan Synchrotron Radiation Research Institute (Proposal No. 2005A0445-CM-np).

*matusita@spring8.or.jp

[1] D. Gabor, Nature (London) **161**, 777 (1948).
[2] A. Szöke, in *Short Wavelength Coherent Radiation: Generation and Applications*, AIP Conf. Proc. No. 147 (AIP, New York, 1986), p. 361.
[3] J. J. Barton, Phys. Rev. Lett. **61**, 1356 (1988).
[4] J. J. Barton, Phys. Rev. Lett. **67**, 3106 (1991).
[5] G. R. Harp, D. K. Saldin, and B. P. Tonner, Phys. Rev. B **42**, 9199 (1990).
[6] H. Takagi, H. Daimon, F. Palomares, and C. S. Fadley, Surf. Sci. **470**, 189 (2001).
[7] S. Y. Tong, C. M. Wei, T. C. Zhao, H. Huang, and H. Li, Phys. Rev. Lett. **66**, 60 (1991).
[8] B. P. Tonner, Zhi-Lan Han, G. R. Harp, and D. K. Saldin, Phys. Rev. B **43**, 14423 (1991).
[9] D. K. Saldin, G. R. Harp, B. L. Chen, and B. P. Tonner, Phys. Rev. B **44**, 2480 (1991).
[10] S. Y. Tong, H. Huang, and C. M. Wei, Phys. Rev. B **46**, 2452 (1992).
[11] L. J. Terminello, J. J. Barton, and D. A. Lapiano-Smith, Phys. Rev. Lett. **70**, 599 (1993).
[12] D. K. Saldin, G. R. Harp, and X. Chen, Phys. Rev. B **48**, 8234 (1993).
[13] H. Wu, G. J. Lapeyre, H. Huang, and S. Y. Tong, Phys. Rev. Lett. **71**, 251 (1993).
[14] S. Y. Tong, H. Li, and H. Huang, Phys. Rev. Lett. **67**, 3102 (1991).
[15] S. Thevuthasan, G. S. Herman, A. P. Kaduwela, R. S. Saiki, Y. J. Kim, W. Niemczura, M. Burger, and C. S. Fadley, Phys. Rev. Lett. **67**, 469 (1991).
[16] G. S. Herman, S. Thevuthasan, T. T. Tran, Y. J. Kim, and C. S. Fadley, Phys. Rev. Lett. **68**, 650 (1992).
[17] H. Wu and G. J. Lapeyre, Phys. Rev. B **51**, 14549 (1995).
[18] D.-A. Luh, T. Miller, and T.-C. Chiang, Phys. Rev. Lett. **81**, 4160 (1998).
[19] P. M. Len, J. D. Denlinger, E. Rotenberg, S. D. Kevan, B. P. Tonner, Y. Chen, M. A. Van Hove, and C. S. Fadley, Phys. Rev. B **59**, 5857 (1999).
[20] J. Wider, F. Baumberger, M. Sambi, R. Gotter, A. Verdini, F. Bruno, D. Cvetko, A. Morgante, T. Greber, and J. Osterwalder, Phys. Rev. Lett. **86**, 2337 (2001).
[21] S. Omori, Y. Nihei, E. Rotenberg, J. D. Denlinger, S. Marchesini, S. D. Kevan, B. P. Tonner, M. A. Van Hove, and C. S. Fadley, Phys. Rev. Lett. **88**, 055504 (2002).
[22] Ph. Hofmann and K.-M. Schindler, Phys. Rev. B **47**, 13941 (1993).
[23] Ph. Hofmann, O. Schaff, and K.-M. Schindler, Phys. Rev. Lett. **76**, 948 (1996).
[24] M. Tegze and G. Faigel, Europhys. Lett. **16**, 41 (1991).
[25] P. M. Len, S. Thevuthasan, C. S. Fadley, A. P. Kaduwela, and M. A. Van Hove, Phys. Rev. B **50**, 11275 (1994).
[26] P. M. Len, T. Gog, D. Novikov, R. A. Eisenhower, G. Materlik, and C. S. Fadley, Phys. Rev. B **56**, 1529 (1997).
[27] T. Gog, P. M. Len, G. Materlik, D. Bahr, C. S. Fadley, and C. Sanchez-Hanke, Phys. Rev. Lett. **76**, 3132 (1996).
[28] S. Marchesini and C. S. Fadley, Phys. Rev. B **67**, 024115 (2003).
[29] S. Omori, L. Zhao, S. Marchesini, M. A. Van Hove, and C. S. Fadley, Phys. Rev. B **65**, 014106 (2001).
[30] K. Hayashi, M. Matsui, Y. Awakura, T. Kaneyoshi, H. Tanida, and M. Ishii, Phys. Rev. B **63**, 041201(R) (2001).
[31] Y. Takahashi, K. Hayashi, and E. Matsubara, Phys. Rev. B **68**, 052103 (2003).
[32] K. Hayashi, T. Hayashi, T. Shishido, E. Matsubara, H. Makino, T. Yao, and T. Matsushita, Phys. Rev. B **76**, 014119 (2007).
[33] T. Matsushita, A. Agui, and A. Yoshigoe, Europhys. Lett. **65**, 207 (2004).
[34] T. Matsushita, A. Yoshigoe, and A. Agui, Europhys. Lett. **71**, 597 (2005).
[35] T. Matsushita, F. Z. Guo, F. Matsui, Y. Kato, and H. Daimon, Phys. Rev. B **75**, 085419 (2007).
[36] F. Matsui, H. Daimon, F. Z. Guo, and T. Matsushita, Appl. Phys. Lett. **85**, 3737 (2004).
[37] H. Daimon, Rev. Sci. Instrum. **59**, 545 (1988).
[38] M. Kotsugi, T. Miyatake, K. Enomoto, K. Fukumoto, A. Kobayashi, T. Nakatani, Y. Saitoh, T. Matsushita, S. Imada, T. Furuhata, S. Suga, K. Soda, M. Jinno, T. Hirano, K. Hattori, and H. Daimon, Nucl. Instrum. Methods Phys. Res. A **467-468**, 1493 (2001).
[39] K. Hirano, K. Izumi, T. Ishikawa, S. Annaka, and S. Kikuta, Jpn. J. Appl. Phys., Part 2 **30**, L407 (1991).
[40] H. Maruyama, M. Suzuki, N. Kawamura, M. Ito, E. Arakawa, J. Kokubun, K. Hirano, K. Horie, S. Uemura, K. Hagiwara, M. Mizumaki, S. Goto, H. Kitamura, K. Namikawa, and T. Ish-

ikawa, J. Synchrotron Radiat. **6**, 1133 (1999).
[41] D. K. Saldin, G. R. Harp, and B. P. Tonner, Phys. Rev. B **45**, 9629 (1992).
[42] G. Faigel and M. Tegze, Rep. Prog. Phys. **62**, 355 (1999).
[43] D. M. Collins, Nature (London) **298**, 49 (1982).
[44] S. Marchesini, N. Mannella, C. S. Fadley, M. A. Van Hove, J. J. Bucher, D. K. Shuh, L. Fabris, M. J. Press, M. W. West, W. C. Stolte, and Z. Hussain, Phys. Rev. B **66**, 094111 (2002).
[45] P. Korecki, M. Tolkiehn, D. V. Novikov, G. Materlik, and M. Szymonski, Phys. Rev. Lett. **96**, 035502 (2006).